

Quantifying the Importance of Ram Pressure Stripping in a Galaxy Group at 100 Mpc

E. Freeland^{1*}, C. Sengupta^{2,3*}, & J. H. Croston^{4*}

¹*George P. & Cynthia W. Mitchell Institute for Fundamental Physics and Astronomy,*

Department of Physics and Astronomy, Texas A&M University, College Station, TX 77843, USA

²*Calar-Alto Observatory, Centro Astronomico Hispano Aleman, C/Jesus Durban Remon, 2-2 04004 Almeria, Spain*

³*Instituto de Astrofísica de Andalucía (CSIC), Glorieta de Astronomía s/n, 18008 Granada, Spain*

⁴*School of Physics and Astronomy, University of Southampton, Southampton, SO17 1SJ, UK*

Accepted 2010 July 17. Received 2010 July 12; in original form 2010 May 14

ABSTRACT

We examine two members of the NGC 4065 group of galaxies: a bent-double (a.k.a. wide angle tail) radio source and an HI deficient spiral galaxy. Models of the X-ray emitting intragroup gas and the bent-double radio source, NGC 4061, are used to probe the density of intergalactic gas in this group. HI observations reveal an asymmetric, truncated distribution of HI in spiral galaxy, UGC 07049, and the accompanying radio continuum emission reveals strong star formation. We examine the effectiveness of ram pressure stripping as a gas removal mechanism and find that it alone cannot account for the HI deficiency that is observed in UGC 07049 unless this galaxy has passed through the core of the group with a velocity of $\sim 800 \text{ km s}^{-1}$. A combination of tidal and ram pressure stripping are necessary to produce the HI deficiency and asymmetry in this galaxy.

Key words: galaxies: groups: individual: NGC 4065 – intergalactic medium – galaxies; jets – galaxies: evolution

1 INTRODUCTION

Galaxy characteristics, like morphology and star-formation rate (SFR), are observed to change with environment where high density regions like clusters are characterized by a larger fraction of elliptical galaxies and a lower star-formation rate than seen in the field (Dressler 1980; Goto et al. 2003; Gómez et al. 2003). These observations are known as the morphology-density and SFR-density relations, although Whitmore et al. (1991,1993) argue that these reflect a tighter and more fundamental morphology-radius relation where the distance from the cluster centre is the independent parameter. The morphology-density relation shows distinct behavior over three separate regimes which can be characterized in terms of the projected galaxy density or the radial distance from the cluster centre (in terms of the virial radius, R_{vir} , defined by the Girardi et al. (1998) as $R_{vir} \simeq 0.002\sigma_r h_{100}^{-1}$ Mpc). In the lowest density regions farthest from cluster centres (with projected densities $< 1 \text{ Mpc}^{-2}$ or radius $> 1 R_{vir}$) the relation is flat, suggesting that the physical mechanisms responsible for changes in morphology are not effective in this regime.

At a characteristic radius of $\sim 1 R_{vir}$ (projected densities of $1 - 6 \text{ Mpc}^{-2}$) the fraction of intermediate type (S0) galaxies begins to increase while the late-type disk (Sc) galaxy fraction decreases and the SFR decreases sharply (Gómez et al. 2003). These trends continue till $\sim 0.3 R_{vir}$ (projected density $> 6 \text{ Mpc}^{-2}$) where the fraction of intermediate types decreases and the elliptical fraction dramatically increases (Goto et al. 2003). The behavior of these relations over the separate regimes indicates a change in the dominant physical mechanisms influencing the evolution of galaxies across these environments.

There are a variety of physical mechanisms that could be responsible for altering galaxy morphology in dense environments, including ram pressure stripping, tidal interactions, galaxy harassment, strangulation, and major and minor mergers. The vast majority of galaxies in the universe reside in groups which are small dynamical systems typically containing a handful of large ($\sim L_*$) galaxies and a large number of smaller galaxies (Geller & Huchra 1983; Tully 1987; Eke 2004; Yang et al. 2007; Tago et al. 2008). These systems have velocity dispersions between $\sim 30 - 500 \text{ km s}^{-1}$ and intragroup medium (IGM) densities that are not well constrained. Thus, it has been thought that tidal interactions are likely to dominate in this envi-

* E-mail: freeland@physics.tamu.edu (EF); chandra@caha.es (CS), J.Croston@soton.ac.uk (JHC)

ronment while ram pressure stripping and strangulation are less likely to be important.

Galaxy groups, according to the hierarchical scenario of the formation of large-scale structure, are the building blocks of rich clusters of galaxies. Since most galaxies exist in groups these are important sites in which to investigate the physical mechanisms responsible for the observed morphology and SFR-density relations. Two important questions arise:

- To what extent are field galaxies and intergalactic gas preprocessed by the group environment before they are incorporated into galaxy clusters?
- Which physical mechanisms are important in altering the morphology and SFR of galaxies in the group environment?

Here we present observations of the NGC 4065 group, located in the Coma Supercluster. This group is a unique laboratory for studying ram pressure stripping as we have two independent means of measuring the density of the intergalactic gas in this system which also contains an HI deficient, edge-on, Sc galaxy (UGC 07049). This group has an average velocity of $6995 \pm 48 \text{ km s}^{-1}$ ($z = 0.0233$), a velocity dispersion of $416 \pm 35 \text{ km s}^{-1}$, and extended X-ray emission from the intragroup medium (Mahdavi & Geller 2004). Our VLA D-array data show numerous interactions among HI rich group members outside of the core of the group (Freeland et al. 2009). Gavazzi et al. (2006) classify UGC 07049 as strongly HI deficient using Arecibo data and find it has a total HI mass of $2 \times 10^9 M_{\odot}$. This group is also known as RASSCAL S NRGb 177 (Mahdavi et al. 2000), GEMS NGC 4065 (Osmond & Ponman 2004), and GH 98 (Geller & Huchra 1983).

At the distance of this group $1'$ corresponds to ~ 30 kpc. We use a Hubble constant of $75 \text{ km s}^{-1} \text{ Mpc}^{-1}$.

2 OBSERVATIONS

2.1 GMRT Data

The NGC 4065 group was observed with the Giant Metrewave Radio Telescope (GMRT) at 610 MHz in the standard continuum observing mode in August of 2007 for 8 hours including calibration. Both the upper and lower sidebands of the correlator were used with 16 MHz bandwidth in each. Here we present only upper sideband data.

The group was observed in HI 21 cm line using the GMRT in May of 2008. At 1420 MHz, the system temperature and the gain (K/Jy) of the instrument are 76K and 0.22 respectively. The observations were carried out in the Indian polar mode. The baseband bandwidth used was 16 MHz, giving a velocity resolution of 27 km s^{-1} . The on source integration time was 15 hours. The pointing centre for the HI observations was $12^{\text{h}} 04^{\text{m}} 01.^{\text{s}}5 + 20^{\circ} 13' 54.34''$ in J2000 co-ordinates.

The radio data were reduced using AIPS (Astronomical Image Processing System) using standard procedures. Bad data due to dead antennas and radio frequency interference (RFI) were flagged and the data were calibrated for amplitude and phase using the primary and secondary calibrators. The primary calibrator was also used as the bandpass calibrator. The 20 cm radio continuum maps were made using

the self calibrated line free channels of the observations. The radio continuum was then subtracted from the data using the AIPS tasks UVSUB and UVLIN. The final 3-dimensional deconvolved HI data cubes were then obtained from the continuum subtracted data using the task IMAGR. From these cubes the total HI images and the HI velocity fields were extracted using the task MOMNT.

2.2 XMM-Newton Data

A short archival *XMM-Newton* observation of the environment of radio source NGC 4061 (observation ID 0112271101, carried out on 2003 June 30th) was used to study the X-ray emission from the intragroup medium. The X-ray data were reprocessed using the *XMM-Newton* SAS version 6.0.0, and the latest calibration files from the *XMM-Newton* website. The pn data were filtered to include only single and double events ($\text{PATTERN} \leq 4$), and $\text{FLAG}==0$, and the MOS data were filtered according to the standard flag and pattern masks ($\text{PATTERN} \leq 12$ and $\#\text{XMMEA_EM}$, excluding bad columns and rows). The dataset was affected by background flares, so filtering for good time intervals was applied to ensure that accurate measurements could be made in low surface-brightness regions. Lightcurves in the 10 – 12 keV (MOS) or 12 – 14 keV (pn) energy bands were used to identify time periods of high background rate, and thresholds of 0.4 cts s^{-1} (MOS) and 0.7 cts s^{-1} (pn) were applied. The exposure times remaining after GTI filtering were 5677 s, 6032 s and 3335 s for the MOS1, MOS2 and pn cameras, respectively.

Spectral and spatial analysis were carried out using the filtered *XMM-Newton* events lists. The background was accounted for accurately using the double subtraction method described in Croston et al. (2008), which makes use of filter-wheel closed datasets to constrain the instrumental and particle components of the background. Both source and background (filter-wheel closed) events lists were vignetting corrected using the SAS task *evigweight*. The background datasets were scaled to account for differences in the level of the instrumental and particle background components using a weighting factor consisting of the ratio of source to background 10 – 12 keV count rate in a large background annulus. For surface brightness profile analysis, a background profile was first obtained by extracting a profile matched to the source profile from the weighted background file. The difference in background level between source and background profiles in the outer regions (where source emission should be negligible) was used as a second background component to subtract off the soft X-ray background from Galactic and cosmic X-ray components. For spectral analysis an equivalent process was used: spectra were obtained from the source and appropriate background events lists for both target and local background extraction regions. The Galactic/cosmic X-ray background contribution was modeled by fitting an X-ray background model to the local background spectrum consisting of two *mekal* models to account for emission from the Galactic bubble and a power-law model absorbed by the Galactic N_H in the direction of the target to account for the cosmic X-ray background. The *mekal* temperatures were allowed to vary, but the power-law index was fixed at $\Gamma = 1.41$ (Lumb et al. 2002). The normalizations of all three components were allowed to vary. For each source spectrum,

we used the corresponding filter-wheel closed spectrum as a background spectrum, to account for particle background, and a fixed X-ray background model consisting of the best-fitting model from the fit to the outer, source-free region, with the normalizations of each component fixed at the best-fitting values scaled to the appropriate area for the source extraction region.

We extracted spectra for the group emission from an annular region of inner radius 2 arcmin (to exclude any AGN-related X-ray emission) and outer radius 6.7 arcmin. The spectra were fitted with a *mekal* model in addition to the fixed X-ray background model as described above. The best-fitting model parameters for a joint fit to the MOS1 and pn spectra in the energy range 0.3 – 7.0 keV were $kT = 1.31^{+0.14}_{-0.23}$ keV and $Z = 0.33^{+0.28}_{-0.19} Z_{\odot}$ using a Galactic $N_{\text{H}} = 2.3 \times 10^{20} \text{ cm}^{-2}$, giving $\chi^2 = 234$ for 186 d.o.f.

Surface brightness profiles were extracted from the MOS1 and pn events lists, which showed evidence for both an inner galaxy-scale halo and a flatter, group-scale component. A single β -model fit to the profiles was therefore a poor fit. We fitted the profiles with the projected double-beta model as described in Croston et al. (2008), which is the surface brightness profile corresponding to a gas density profile of:

$$n(r) = n_0 \left[\left(1 + \frac{r^2}{r_{c,in}^2} \right)^{-3\beta_{in}/2} + N \left(1 + \frac{r^2}{r_c^2} \right)^{-3\beta/2} \right] \quad (1)$$

where N is the relative normalization of the two β model component. Before fitting, each model was convolved with the *XMM-Newton* PSF based on the on-axis parameterization described in the *XMM-Newton* CCF files XRT1_XPSF_0006.CCF, XRT2_XPSF_0007.CCF and XRT3_XPSF_0007.CCF. The Markov-Chain Monte Carlo (MCMC) method for exploring the 6-dimensional parameter space for this model described in Croston et al. (2008) was used to determine the best fitting model parameters for the gas density profile, with the joint χ^2 value for the three profiles as the likelihood estimator. Plausible ranges for each parameter were estimated by carrying out extreme fits and these were used as priors for the MCMC method. Quantities derived from the surface brightness model fits, including X-ray luminosity and pressure at a given radius, are obtained by determining that quantity for each model fit and then obtaining the Bayesian estimate for the quantity in question. Uncertainties on the derived quantities are the minimal 1-dimensional interval enclosing 68 per cent of the values for the given quantity, and so correspond to the 1σ intervals for one interesting parameter. Some of the parameters are strongly correlated, leading to large uncertainties on the individual model parameters; however, tight constraints can be obtained on derived quantities such as pressure and luminosity. The best-fitting model parameters were $\beta_{in} = 1.2$, $r_{c,in} = 13.1$ arcsec, $\beta = 1.2$, $r_c = 256$ arcsec, and $N = 0.02453$ with $\chi^2 = 24.4$ for 16 d.o.f. Figure 1 shows the number density profile for the hot intergalactic gas in the core of this group.

3 GROUP DYNAMICS

We rely on the redshift survey of this group performed by Mahdavi & Geller (2004) which finds 74 members with an

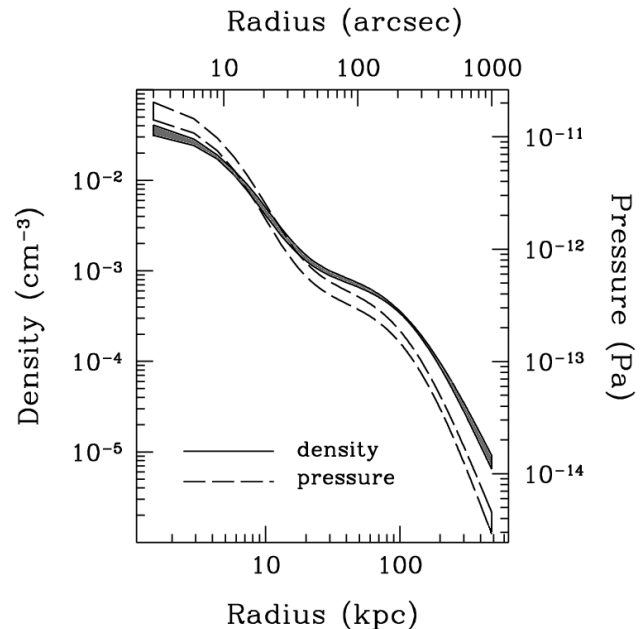


Figure 1. Number density and pressure profiles from the model fits to the *XMM-Newton* data showing the X-ray emitting gas in this group. The pressure profile is calculated from the density profile assuming temperature, $kT = 1.31$ keV. Uncertainties (1σ) in the density and pressure are illustrated by the width of the curves.

average velocity of $6995 \pm 48 \text{ km s}^{-1}$ and a velocity dispersion of $416 \pm 35 \text{ km s}^{-1}$. The group has two compact subgroups, UZG-CG 156 (including NGC 4076) and UZC-CG 157 (including NGC 4061), which were identified by the 3D Updated Zwicky Catalog (Falco et al. 1999) solely on the criterion of compactness (Focardi & Kelm 2002). These two subgroups are not distinguishable by velocity. However, there does appear to be an extended tail in the distribution toward lower velocities. The galaxies in this extended tail are clustered on the sky near UZC-CG 156 and may represent a filament toward nearby ($\sim 6^\circ$ away) rich cluster Abell 1367 whose velocity is 6595 km s^{-1} .

If we assume that the extended tail is not significantly dynamically associated with the NGC 4065 group, and we remove those velocities from the sample, then the velocity dispersion becomes $220 \pm 30 \text{ km s}^{-1}$. The errors on this velocity dispersion are determined by generating bootstrap samples.

The lack of simple gaussianity in the distribution of velocities and the strong spatial bimodality in the diffuse X-ray emission indicates that the system is not in dynamical equilibrium. If we assume that group potential is deepest at the peak of the velocity histogram then the X-ray gas of this peak is located at a velocity of $\sim 7150 \text{ km s}^{-1}$. The velocity of NGC 4065 ($v = 6326 \text{ km s}^{-1}$), the early-type galaxy immediately east of radio galaxy NGC 4061, puts it likely outside of the core of the group despite its projected appearance. The velocity of bent-double radio galaxy, NGC 4061, as measured by Mahdavi & Geller (2004) is $7393 \pm 32 \text{ km s}^{-1}$. Previous radial velocity measurements have given this source a velocity of $7203 \pm 27 \text{ km s}^{-1}$ (de Vaucouleurs et al. 1991) and $7369 \pm 52 \text{ km s}^{-1}$ (Falco et al. 1999).

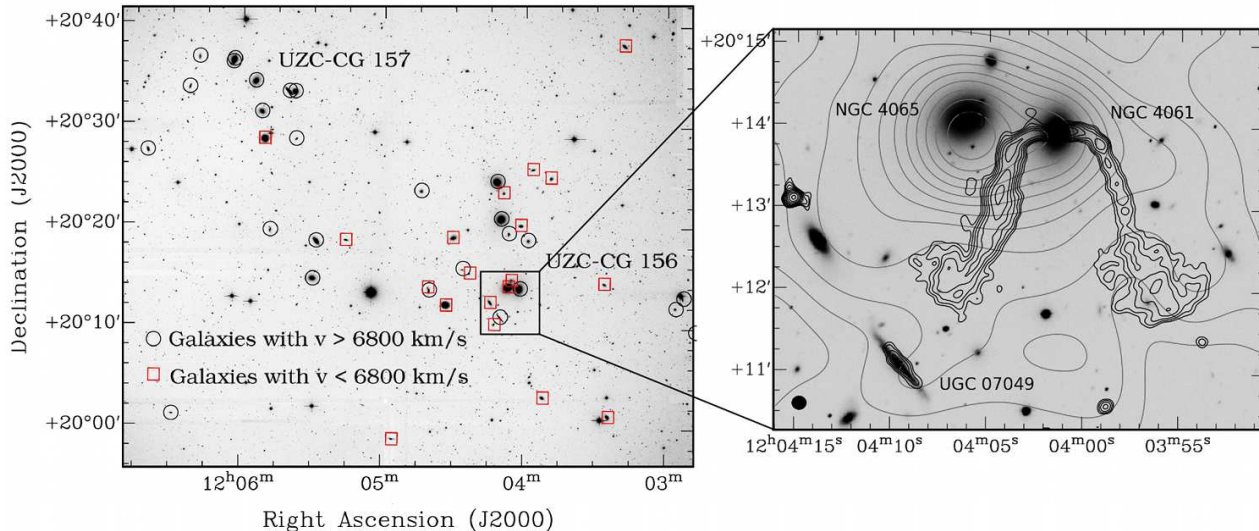


Figure 3. *Left:* The spatial locations of galaxies with recessional velocities greater than 6800 km s^{-1} are marked with black circles. The spatial locations of galaxies with recessional velocities less than 6800 km s^{-1} are marked with red squares. The underlying image was taken in the optical R band. There are approximately 20 more galaxies identified as group members by Mahdavi & Geller (2004) which are beyond the edge of the optical image, mainly to the north and west. *Right:* XMM X-ray (grey) and GMRT 60cm radio continuum (black) contours overlaid on an optical R band image of the core of the NGC 4065 galaxy group, also the core of compact subgroup UZC-CG 156. Radio continuum emission from the disk of spiral galaxy UGC 07049 indicates it has a high star formation rate. The 60cm radio contours start at $1.4 \text{ mJy beam}^{-1}$ and increase by $\sqrt{2}$. The $7.8'' \times 6.7''$ 60cm beam is shown in the lower left corner. At the distance of this group $1'$ corresponds to 30 kpc.

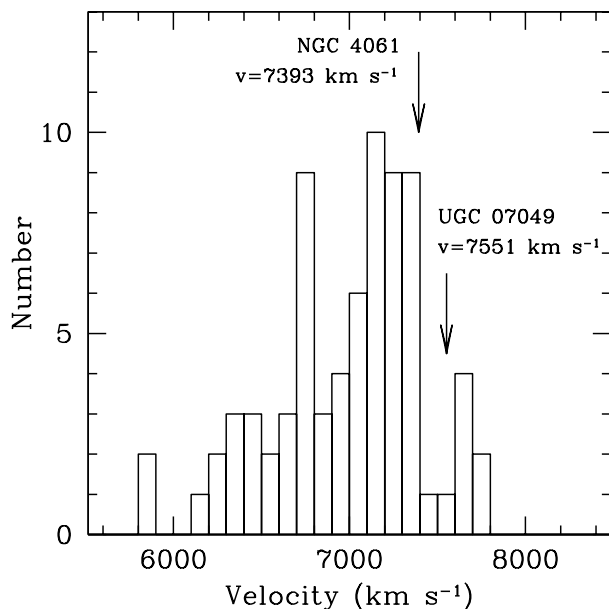


Figure 2. Histogram of velocities for the NGC 4065 group of galaxies from the data in Mahdavi & Geller (2004). The velocity of bent-double radio source NGC 4061 and that of spiral galaxy UGC 07049 are indicated with arrows. The bins are 100 km s^{-1} wide.

4 BENT-DOUBLE RADIO SOURCE NGC 4061

We follow the method for using bent-double radio sources as probes of intergalactic gas outlined in Freeland et al. (2008) with a few additional caveats. We are assuming that the

jet bulk flows have decelerated to non-relativistic speeds on kilo-parsec scales, and certainly by the time they are bent by the motion of the host galaxy ($\sim 15 \text{ kpc}$ from the core of the radio galaxy). This assumption is borne out by the symmetric fluxes in the two jets (see Figure 3), were they still relativistic then beaming effects would produce asymmetric fluxes which would be easily observable in these data. We also consider additional pressure in the jets from entrained material.

Bent-double radio sources can be used to measure the density of intergalactic gas by the application of Euler's equation (Begelman et al. 1979; Jones & Owen 1979; Burns & Owen 1980). The time-independent Euler equation describes the balance of internal and external pressure gradients,

$$\frac{\rho_{\text{IGM}} v_{\text{gal}}^2}{h} = \frac{\rho_j v_j^2}{R} \quad (2)$$

where $\rho_{\text{IGM}} v_{\text{gal}}^2$ is the external ram pressure felt by the radio galaxy as it travels through the IGM, $\rho_j v_j^2$ is the internal pressure of the jet, h is the width of the jet, and R is the radius of curvature of the jet. We estimate the speed of the radio galaxy using the group velocity dispersion. The pressure in the jets is determined at a position in the jet immediately before it bends using the minimum synchrotron pressure as outlined in O'Dea & Owen (1987). Standard equipartition of energy between relativistic particles and magnetic fields is assumed. We assume a radio spectral index of $\alpha = 0.55$ in the jets through the point where they bend as is seen in other FRI sources with high-resolution, multi-frequency radio data (Laing et al. 2008; Young et al. 2005). Our values for the minimum synchrotron pressure in the jets are in good agreement with other mea-

measurements for similar radio sources (Venkatesan et al. 1994; Worrall & Birkinshaw 2000).

Observations of straight FRI sources show that the minimum synchrotron pressure in the jets does not balance the observed external pressure from the intergalactic gas as measured by modeling its X-ray emission (Bicknell 1984; Laing & Bridle 2002; Croston et al. 2008). The standard assumption is that entrained thermal protons are likely responsible for the additional energy density above that provided by the relativistic particles and magnetic fields in the jets. This entrained material must have a lower temperature than the surrounding hot gas because the X-ray surface brightness decreases at the locations of the radio lobes (e.g. Croston et al. 2003). Here we consider both the case without entrained material and the case where entrained material provides five times the energy density of the relativistic electrons. The ratio of energy density between the relativistic electrons and the entrained material is not well constrained, however, a factor of five is typical on scales of 15 – 20 kpc (Croston & Hardcastle 2010 *in prep*).

We find an intergalactic gas density of $2 \pm 0.5 \times 10^{-27} \text{ g cm}^{-3}$ or $2 \pm 0.5 \times 10^{-3} \text{ cm}^{-3}$ when entrained thermal protons provide additional internal pressure in the jets. With the standard equipartition minimum synchrotron pressure from relativistic electrons only, the density of the intergalactic gas that NGC 4061 is traveling through is $4 \pm 1 \times 10^{-28} \text{ g cm}^{-3}$ or $4 \pm 1 \times 10^{-4} \text{ cm}^{-3}$. This intergalactic gas density, for the case including entrained protons, is very similar to the density in the model fit to the X-ray emitting intergalactic gas at the projected position of NGC 4061 (~ 30 kpc from the X-ray centre). We have good reason to believe that NGC 4061 is located within the X-ray emitting gas because the X-ray contours trace the flaring ends of the jets very closely.

5 STAR-FORMING GALAXY UGC 07049

UGC 07049 is a late type spiral at an angular distance of $3.4'$ from NGC4061. It has a radial velocity of 7551 km s^{-1} and is of the morphological type Sc. As has been mentioned earlier, this galaxy shows significant HI deficiency. Additionally, it may be traveling through the X-ray emitting hot gas in the core of this group which makes it an interesting target in which to study how a hot IGM affects the neutral gas content of spiral galaxies.

5.1 HI Content and Distribution

Figure 6 shows a high resolution ($15'' \times 15''$) HI column density image of UGC 07049 overlaid on an optical R band image. The HI distribution in the disk is asymmetric, with a peak in the HI south of the centre of the galaxy. A distinct feature is that the HI disk is similar in extent to the optical disk. In normal late type spirals of similar morphological type, typical HI disks are found to be 1.5 to 2 times larger in extent than the optical disk (Broeils & Rhee 1997). Figure 5 shows the interferometric HI spectrum of UGC 07049 from our GMRT data. The integrated flux density as estimated from this spectrum is $0.86 \text{ Jy km s}^{-1}$, which matches well with the single dish value reported in Huchtmeier & Richter (1989) ($0.85 \text{ Jy km s}^{-1}$) and is

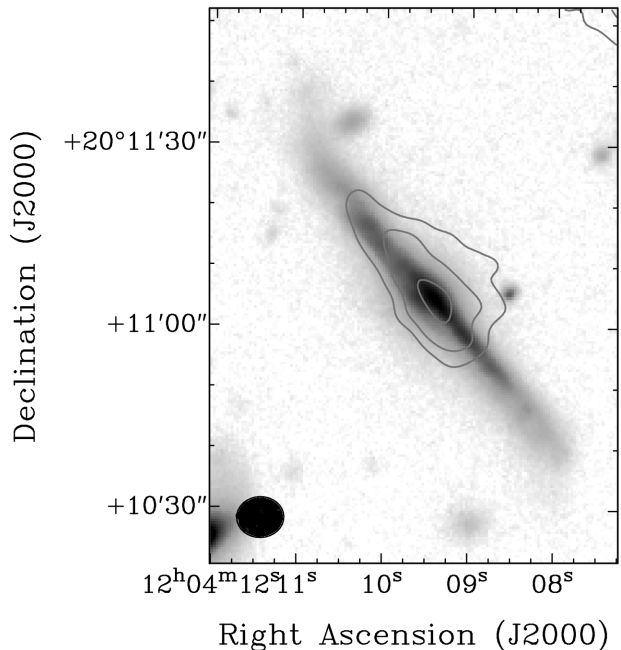


Figure 4. 20 cm radio continuum emission from UGC 07049 shown as contours on an optical R band image. The lowest contour is $0.8 \text{ mJy beam}^{-1}$ and contours increase by $\sqrt{2}$. The beam is shown in the lower left corner of the image. This emission is the result of star formation in the disk of the galaxy.

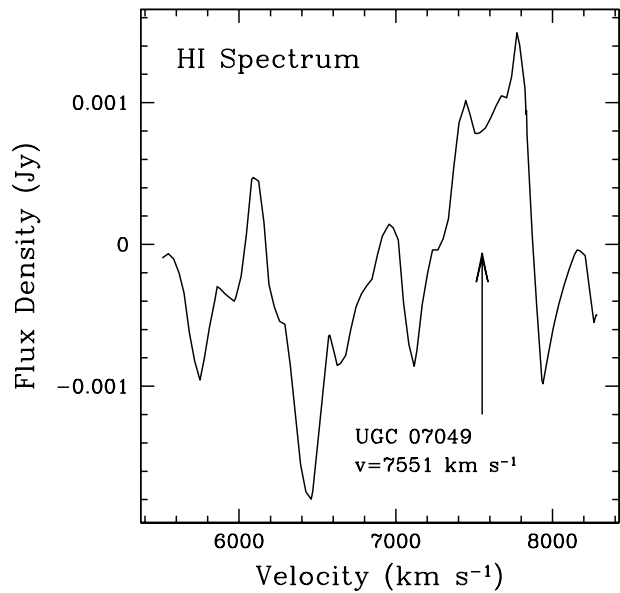


Figure 5. Interferometric HI spectrum of UGC 07049 from our GMRT data.

slightly lower than that reported from Arecibo observations by Springob et al. (2005) ($1.12 \text{ Jy km s}^{-1}$). The $0.86 \text{ Jy km s}^{-1}$ integrated flux density corresponds to an HI mass of $2 \times 10^9 M_{\odot}$. A reasonable match of the integrated line flux densities of GMRT data and single dish observations imply

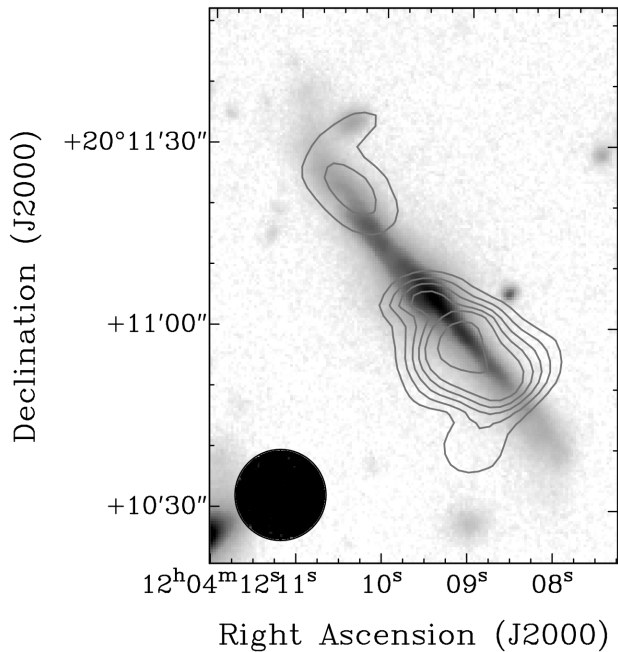


Figure 6. High resolution (15'') total HI contours for UGC07049 overlaid on an optical R band image. The HI column density contour levels are $8.3 \times 10^{19} \times (3, 5, 7, 9, 11, 15, 20)$.

that we have not lost any diffuse extended emission and the HI disk is indeed similar in size as the optical disk.

The parameter that indicates whether a galaxy has lost gas compared to a field galaxy of similar size and similar morphological type is typically known as the ‘HI deficiency’ and is given by

$$def_{HI} = \log \frac{M_{HI}}{D_l^2} |_{predicted} - \log \frac{M_{HI}}{D_l^2} |_{observed} \quad (3)$$

where M_{HI} is the total HI mass of a galaxy and D_l is the optical major isophotal diameter (in kpc) measured at or reduced to a surface brightness level $m_B = 25.0$ mag/arcsec².

The ‘predicted’ field galaxy value of HI surface density for morphological type Sc has been taken from Haynes & Giovanelli (1984). While Haynes & Giovanelli (1984) used the UGC blue major diameters for D_l , in this work RC3 major diameter have been used. To take care of the difference in the surface matter density that result from the use of RC3 diameters, a value of 0.08 (de Vaucouleurs et al. 1991) has been added to the predicted surface density given by Haynes & Giovanelli (1984). Assuming a distance of 100.7 Mpc, derived using the optical velocity of UGC 07049 and using its RC3 diameter value 0.91', the HI deficiency of the galaxy is found to be ~ 0.41 . This implies that the galaxy is ~ 2.6 times deficient in HI.

5.2 Ram Pressure Stripping

Possible causes for the HI deficiency include tidal interactions, ram pressure stripping, or a combination of these two processes. In the HI images we do not see any HI tidal extensions, although the stellar disk appears to be warped on the north-east end. Recent studies have shown that in groups with X-ray bright IGM ram pressure alone

or tidally aided ram pressure is capable of removing a considerable fraction of the gas from constituent galaxies (Sengupta et al. 2007; Sengupta & Balasubramanyam 2006; Rasmussen et al. 2006; Davis et al. 1997). The HI data presented here show the gaseous disk of UGC 07049 to be of similar size to the optical disk, whereas normal galaxies are known to have larger HI disks compared to their optical disks. Truncated HI disks are common in clusters of galaxies and in many cases are thought to result from ram pressure stripping. The low column density gas from the outer edges of the disk is swept out by the ram pressure offered by the dense intracluster gas, leaving behind a reduced HI disk.

The NGC 4065 group has been detected to have a hot IGM and also a bent radio jet indicating resistance from the IGM. The spiral UGC 07049 is located within the projected X-ray emitting gas. Using some simple calculations we will explore whether ram pressure in this group is strong enough to strip gas from UGC 07049. We have followed the method outlined in Sengupta et al. (2007) for calculating the possible gas loss from UGC 07049 due to ram pressure.

Ram pressure stripping will be effective for a galaxy when the HI surface density, σ_μ , is less than $\rho_{IGM} v_{gal}^2 / (2\pi G \sigma_*)$, where σ_* is the stellar surface density, ρ_{IGM} is the local IGM density and v_{gal} is the velocity with which the galaxy is moving through the medium. We use the local projected IGM density of 4×10^{-4} cm⁻³ from the X-ray gas profile, and for the velocity of UGC 07049 we consider both the 220 km s⁻¹ and 416 km s⁻¹ velocity dispersion. The stellar surface density for UGC 07049 is estimated from its 2MASS K-band magnitude and K-J color. Relating the mass to light ratio in the K band (M/L_K) to the K-J colors (Bell & de Jong 2001) along with the relation of L_K to the absolute magnitude in K-band (M_K) (Worthey 1994), we estimate the stellar surface density to be 0.0194 gm cm⁻². With this value for σ_* , the critical HI surface density σ_μ beyond which ram pressure can strip gas off the galaxy, is estimated to be 3.8×10^{-5} gcm⁻² or 2.3×10^{19} cm⁻². We assume the HI surface density distribution inside UGC 07049 to be of constant thickness and with a Gaussian profile (Chamaraux et al. 1980),

$$\sigma(r) = \sigma_0 2^{-r^2/r_H^2} \quad (4)$$

where r_H is the radius within which half the HI mass is present. For σ_0 an average value of 20 M_⊙ pc⁻², as seen in normal late type spirals (Omar & Dwarkanath 2005) in group environments was used. The central HI column density of UGC 07049 also could have been used but the disk was too disturbed and there was a central HI depletion in the high resolution map and thus the map was not used for estimating the σ_0 value. Integrating the surface density distribution to equal the entire observed HI mass allows us to solve for r_H and find a value of 5 kpc. The radius corresponding to σ_μ is then 10 kpc (for the case where $v_{gal} = 416$ km s⁻¹). Finally the HI mass outside this radius, which would be able to be ram pressure stripped, was estimated to be 7×10^7 M_⊙. A similar estimate of the stripped HI mass was done with the 220 km s⁻¹ velocity dispersion and, understandably, produced a smaller mass loss. These calculations assume the galaxy is traveling face-on through the IGM and they do not take into account any of the galaxy’s orbital history.

Compared to the observed HI deficiency the amount

of ram pressure stripped HI is very small, indicating that under the assumed criteria ram pressure alone would not contribute to gas loss in a significant way. However, tidal interactions have been observed to remove large amounts of HI gas from galaxies in groups (Freeland et al. 2009) and can increase the effectiveness of ram pressure stripping. In this scenario, tidal interactions may disturb the gas disk, pull gas out, and reduce the column density enabling even weak ram pressure to strip off low column density gas in large quantities. It is quite possible that UGC 07049 has undergone such stripping in this group given the richness of the system, a hostile X-ray emitting dense IGM, lower than normal gas content, a truncated and asymmetric HI disk, and the disturbed stellar disk. In addition to these, the possibility of this galaxy to have passed through the group core and thereby experience a higher IGM density cannot be ruled out. A trip through the core of this group, experiencing intergalactic gas densities nearly ten times higher, can ram pressure strip enough HI gas to explain the deficiency only if the galaxy velocity is as high as $\sim 800 \text{ km s}^{-1}$.

5.3 Star Formation Rate

UGC 07049 has a 1420 MHz radio continuum flux density of 10.9 mJy. At a distance of 100.7 Mpc this corresponds to an upper limit on the star formation rate of $7 M_{\odot} \text{ yr}^{-1}$ using the simple relation in Yun et al. (2001). This assumes a Salpeter initial mass function integrated over stars with masses ranging from $0.1 M_{\odot}$ to $100 M_{\odot}$.

With a measured HI mass of $2 \times 10^9 M_{\odot}$ and a star formation rate of $7 M_{\odot} \text{ yr}^{-1}$, UGC 07049 will exhaust its HI gas in $\sim 300 \text{ Myr}$. For comparison, the crossing time for this group, assuming a diameter of 1 Mpc, is $\sim 2 \text{ Gyr}$. Thus, the HI deficiency seen in UGC 07049 may also be a result of an elevated star formation rate.

6 SUMMARY

We examine two objects in the NGC 4065 group of galaxies: a bent-double radio source and an HI deficient spiral galaxy. We use X-ray observations and the bent-double radio source to probe the density of intergalactic gas in this group. For the HI deficient spiral, UGC 07049, we calculate the effectiveness of ram pressure stripping as a gas removal mechanism and find that it alone is not strong enough to produce the amount of deficiency that is observed. An elevated star-formation rate is also observed in this galaxy. A combination of tidal and ram pressure stripping, with help from the elevated star-formation rate, are likely strong enough to produce the observed HI deficiency.

ACKNOWLEDGMENTS

We thank the staff of the GMRT who have made these observations possible. GMRT is run by the National Centre for Radio Astrophysics of the Tata Institute of Fundamental Research. This research has made use of the NASA/IPAC extragalactic database (NED) which is operated by the Jet Propulsion Laboratory, Caltech, under contract with the National Aeronautics and Space Administration.

REFERENCES

- Begelman M. C., Rees M. J., Blandford R. D., 1979, *Nat*, 279, 770
- Bell E. F., de Jong R. S., 2001, *ApJ*, 550, 212
- Bicknell G. V., 1984, *ApJ*, 286, 68
- Broeils A. H., Rhee M., 1997, *A&A*, 324, 877
- Burns J. O., Owen F. N., 1980, *AJ*, 85, 204
- Chamaraux P., Balkowski C., Gerard E., 1980, *A&A*, 83, 38
- Croston J. H., Hardcastle M. J., Birkinshaw M., Worrall D. M., 2003, *MNRAS*, 346, 1041
- Croston J. H., Hardcastle M. J., Birkinshaw M., Worrall D. M., Laing R. A., 2008, *MNRAS*, 386, 1709
- Davis D. S., Keel W. C., Mulchaey J. S., Henning P. A., 1997, *AJ*, 114, 613
- de Vaucouleurs G., de Vaucouleurs A., Corwin Jr. H. G., Buta R. J., Paturel G., Fouque P., 1991, *Third Reference Catalogue of Bright Galaxies. Volume 1-3, XII*, 2069 pp. 7 figs.. Springer-Verlag Berlin Heidelberg New York
- Dressler A., 1980, *ApJ*, 236, 351
- Eke V. R. e. a., 2004, *MNRAS*, 348, 866
- Falco E. E., Kurtz M. J., Geller M. J., Huchra J. P., Peters J., Berlind P., Mink D. J., Tokarz S. P., Elwell B., 1999, *PASP*, 111, 438
- Focardi P., Kelm B., 2002, *A&A*, 391, 35
- Freeland E., Cardoso R. F., Wilcots E., 2008, *ApJ*, 685, 858
- Freeland E., Stilp A., Wilcots E., 2009, *AJ*, 138, 295
- Gavazzi G., O'Neil K., Boselli A., van Driel W., 2006, *A&A*, 449, 929
- Geller M. J., Huchra J. P., 1983, *ApJS*, 52, 61
- Girardi M., Giuricin G., Mardirossian F., Mezzetti M., Boschin W., 1998, *ApJ*, 505, 74
- Gómez P. L., Nichol R. C., Miller C. J., Balogh M. L., Goto T., Zabludoff A. I., Romer A. K., Bernardi M., Sheth R., Hopkins A. M., Castander F. J., Connolly A. J., Schneider D. P., Brinkmann J., Lamb D. Q., SubbaRao M., York D. G., 2003, *ApJ*, 584, 210
- Goto T., Yamauchi C., Fujita Y., Okamura S., Sekiguchi M., Smail I., Bernardi M., Gomez P. L., 2003, *MNRAS*, 346, 601
- Haynes M. P., Giovanelli R., 1984, *AJ*, 89, 758
- Huchtmeier W. K., Richter O.-G., 1989, *A General Catalog of HI Observations of Galaxies. The Reference Catalog.. A General Catalog of HI Observations of Galaxies. The Reference Catalog, XIX*, 350 pp. 8 figs.. Springer-Verlag Berlin Heidelberg New York
- Jones T. W., Owen F. N., 1979, *ApJ*, 234, 818
- Laing R. A., Bridle A. H., 2002, *MNRAS*, 336, 1161
- Laing R. A., Bridle A. H., Cotton W. D., Worrall D. M., Birkinshaw M., 2008, in Rector T. A., De Young D. S., eds, *Extragalactic Jets: Theory and Observation from Radio to Gamma Ray Vol. 386 of Astronomical Society of the Pacific Conference Series, Jet Spectra in FRI Radio Galaxies: Implications for Particle Acceleration*. pp 110–+
- Lumb D. H., Warwick R. S., Page M., De Luca A., 2002, *A&A*, 389, 93
- Mahdavi A., Böhringer H., Geller M. J., Ramella M., 2000, *ApJ*, 534, 114
- Mahdavi A., Geller M. J., 2004, *ApJ*, 607, 202
- O'Dea C. P., Owen F. N., 1987, *ApJ*, 316, 95

- Omar A., Dwarakanath K. S., 2005, *JA&A*, 26, 34
Osmond J. P. F., Ponman T. J., 2004, *MNRAS*, 350, 1511
Rasmussen J., Ponman T. J., Mulchaey J. S., 2006, *MNRAS*, 370, 453
Sengupta C., Balasubramanyam R., 2006, *MNRAS*, 369, 360
Sengupta C., Balasubramanyam R., Dwarakanath K. S., 2007, *MNRAS*, 378, 137
Springob, C. M., Haynes, M. P., Giovanelli, R., Kent, B. R., 2005, *ApJS*, 160, 149
Tago E., Einasto J., Saar E., Tempel E., Einasto M., Vennik J., Müller V., 2008, *A&A*, 479, 927
Tully R. B., 1987, *ApJ*, 321, 280
Venkatesan T. C. A., Batuski D. J., Hanisch R. J., Burns J. O., 1994, *ApJ*, 436, 67
Worrall D. M., Birkinshaw M., 2000, *ApJ*, 530, 719
Worthey G., 1994, *ApJS*, 95, 107
Yang X., Mo H. J., van den Bosch F. C., Pasquali A., Li C., Barden M., 2007, *ApJ*, 671, 153
Young A., Rudnick L., Katz D., DeLaney T., Kassim N. E., Makishima K., 2005, *ApJ*, 626, 748
Yun M. S., Reddy N. A., Condon J. J., 2001, *ApJ*, 554, 803

This paper has been typeset from a \LaTeX file prepared by the author.